Coupled Systems Mechanics, *Vol. 7, No. 5 (2018) 555-581*
DOI: https://doi.org/10.12989/csm.2018.7.5.555

Coupled testing-modeling approach to ultimate state computation of steel structure with connections for statics and dynamics

Ismar Imamovic[1,2], Adnan Ibrahimbegovic[*1] and Esad Mesic[2]

[1]*Laboratoire Roberval, Université de Technologie de Compiègne / Sorbonne Universités, France*
[2]*Faculty of Civil Engineering, University Sarajevo, Sarajevo, Bosnia and Herzegovina*

(Received May 29, 2018, Revised June 13, 2018, Accepted June 14, 2018)

Abstract. The moment-resistant steel frames are frequently used as a load-bearing structure of buildings. Global response of a moment-resistant frame structure strongly depends on connections behavior, which can significantly influence the response and load-bearing capacity of a steel frame structure. The analysis of a steel frame with included joints behavior is the main focus of this work. In particular, we analyze the behavior of two connection types through experimental tests, and we propose numerical beam model capable of representing connection behavior. The six experimental tests, under monotonic and cyclic loading, are performed for two different types of structural connections: end plate connection with an extended plate and end plate connection. The proposed damage-plasticity model of Reissner beam is able to capture both hardening and softening response under monotonic and cyclic loading. This model has 18 constitutive parameters, whose identification requires an elaborate procedure, which we illustrate in this work. We also present appropriate loading program and arrangement of measuring equipment, which is crucial for successful identification of constitutive parameters. Finally, throughout several practical examples, we illustrate that the steel structure connections are very important for correct prediction of the global steel frame structure response.

Keywords: steel frame structures; connection behavior; end plate connection; parameters identification

1. Introduction

The moment-resistant steel frame is frequently used as a bearing structure, especially in seismic regions. They provide a very ductile response and a large potential to dissipate energy, which is crucial in the case of earthquakes. These characteristics provide the economical design of the structure and increase resistance with respect to the seismic security. Structural connections between beams and columns play a crucial role in the response of a steel frame structure. They can significantly change the response of the structure, sometimes up to 20%.

∗Corresponding author, Ph.D., E-mail: imamovic.ismar@gmail.com
[a]Professor, E-mail: adnan.ibrahimbegovic@utc.fr
[b]Professor, E-mail: esad_mesic@yahoo.com

http://www.techno-press.org/?journal=csm&subpage=8 ISSN: 2234-2184 (Print), 2234-2192 (Online)

The analysis of a steel structure with connection behavior can be performed with many nonlinear FEM commercial programs, using 3D solid finite elements. The refined nonlinear model can predict the behavior of a joint, but those computations are often too costly and not practical for the design of the whole structure. For this reason, we propose the use of beam element as a better choice regarding computational efficiency and reduced costs. It is well known that geometrically nonlinear elastoplastic beam elements are able to represent the behavior of a steel structure including material nonlinearities and buckling (Imamovic *et al*. 2017, Dujc *et al*. 2010). In this work, we postulate that every connection in steel frame structure can be modeled with beam element. The geometrically nonlinear beam element with bilinear hardening and the linear softening response is used in representing connection behavior. For the modeling of steel members, a simpler beam element with linear hardening and softening is proposed. The constitutive parameters of the beam element are determined from the connection behavior of steel bulk material. The constitutive model we propose is much more refined than the bilinear plasticity model proposed in EC 3 (EC3 2005), where after reaching an ultimate bending moment, the connection response corresponds to perfect plasticity model with a constant value that remains permanently. The EC 3 connection does not consider the shear response and response under cyclic loading. The main novelty of the proposed beam model for representation of the connection behavior is to be able to capture bending and shearing inelastic response with both hardening and softening response (under monotonic and cyclic loading) until the complete failure is reached.

The proposed Reissner beam model contains 18 constitutive parameters that need to be identified. The parameters identification represents a challenge, which can be raised by done using well-designed experimental tests of a structural connection. In this work, experimental testing related to loading program and measurement equipment is designed according to (Imamovic *et al*. 2015). The loading program was defined as cycles of a loading/unloading for the load applied in one direction and as the cyclic load applied in two directions. The measurements were split into the set of local and the set of global measurements. Such experimental testing gives us sufficient information for the identification of the eighteen constitutive parameters. Six experimental tests were performed for two different connection types: end plate connection with the extended plate and end plate connection. The testing structures were designed so that the joint represents the weakest element of the structure.

The outline of the paper is as follows. In the next section, we describe the experimental testing methodology and present main experimental results. The third section gives a brief overview of the main ingredients of the proposed beam model and corresponding FEM implementation. The constitutive parameters identification of the proposed beam element is shown in the fourth section. In the fifth section, we present results of three numerical simulations of the steel frame structures with and without included connection behavior. The last section contains the conclusions.

2. The experimental testing of structural connections

Experimental tests on two types of moment-resistant connection have been conducted with the aim to identify constitutive parameters of the proposed beam model. The tested moment-resistant connection types are: end plate connection with the extended plate and end plate connection. In the experimental structures, connection represents the weakest element where plastic deformations and failure are expected to occur. The vertical and the horizontal beams, chosen as IPE 200 and IPE 400, respectively, are deemed sufficiently strong to remain linear elastic throughout the loading

program.

In total, six experimental tests have been performed. Every connection type has been tested for two different bolt classes (10.9. and 8.8.), while the third test has been conducted under cyclic loading. The experimental tests were performed at the Laboratory for materials and structures of the University of Sarajevo.

According to EC3, the difference in bolt classes should result in different failure mechanisms. EC3 predicts failure in the T-stub (Abidelah *et al*. 2014) for the higher class bolts, and the failure in bolts for the lower class bolts (EC3 2005).

2.1 Experimental setup

Fig. 1 shows the experimental setup for testing connection between two orthogonal steel beams. The equipment for displacements measurements is arranged so that sufficient information for identification of constitutive parameters can be obtained. The experimental data can be classified as the local and the global measurements. The global measurements depend mainly on all model parameters, while the local measurements depend on only one model parameter.

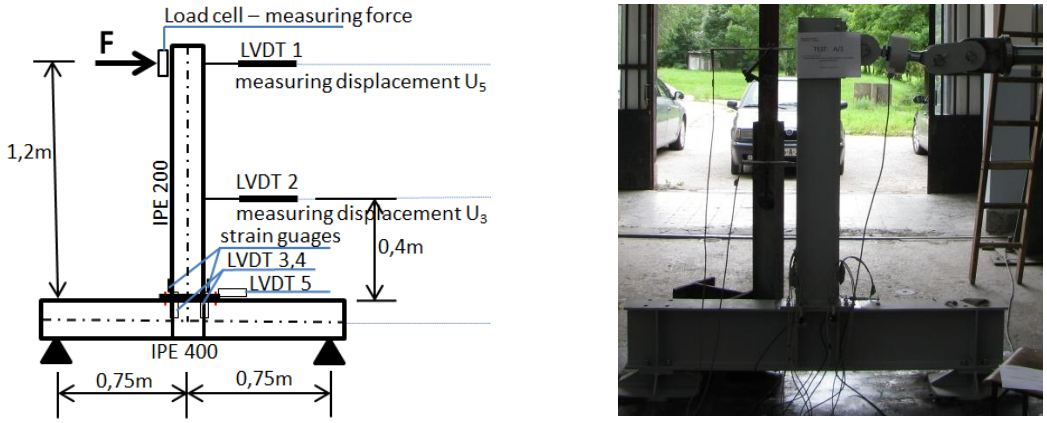

Fig. 1 Experimental setup

The Fig. 1(a) illustrates the measuring equipment, where LVDT is an abbreviation for the "Linear variable displacement transducer", which measures displacements. The LVDT 1 and 2 measure horizontal displacements of the vertical beam ($U_{3,Pi}^{\exp}$) and ($U_{5,Pi}^{\exp}$), which can be classified as the global measurements. All other measurements can be classified as the local. LVDT 3 and 4 are put in vertical position, so that top side is glued to the flange of the vertical beam, and the bottom side is glued to vertical stiffener (see Fig. 2(a)). These LVTD's measure relative vertical displacement between the horizontal beam and the vertical beam, which we use for calculating the rotation of the connection

$$\psi^{\exp} = \frac{\Delta v_3^{\exp} - \Delta v_4^{\exp}}{h_{vert.beam}} \tag{1}$$

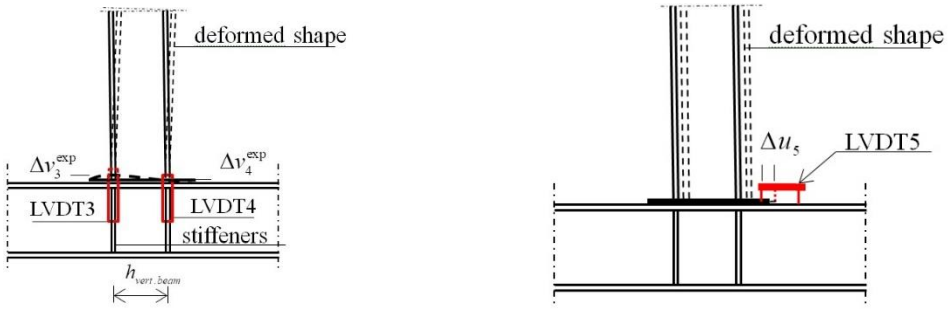

(a) Rotation measurement (b) Shear displacement measurement

Fig. 2 Measuring equipment

LVDT 5 is put in horizontal position, so that left side is glued to the top of steel plate, which is welded to vertical beam, while the right side is glued to the top of horizontal beam (see Fig. 2(b)). This LVDT measures relative horizontal displacement ($U_{2,Pi}^{exp} = U_{S,Pi}^{exp} = \Delta u_5$) between horizontal and vertical beams, which corresponds to transverse (shearing) displacement of the connection.

The strain gauges are put at flanges of the vertical beam, that measure vertical deformation in outer faces, which we use for calculating the curvature of the section near to the connection

$$\varepsilon_i^{exp} = -y \cdot \kappa_i \Rightarrow \kappa_i = -\frac{\varepsilon_i^{exp}}{y};\ y = \left[-\frac{h}{2}, \frac{h}{2}\right] \Rightarrow \kappa^{exp} = \frac{\kappa_1 + \kappa_2}{2} \tag{2}$$

The force F is applied by using a hydraulic pump. The value of the force is measured with load cell placed between the hydraulic pump and the loading point, at the experimental structure. The measuring equipment is controlled with experimental device *Spider 8* and monitored with software *Catman* 5.

Table 1 Geometrical characteristics of experimental structures

Joint	Vertical beam	Horizontal beam	End plate dimension/Angles	Bolts
A1, A3	IPE 200 – S275	IPE 400 – S275	≠ 340×130×10 – S275	8M12-class 8.8.
A2	IPE 200 – S275	IPE 400 – S275	≠ 340×130×10 – S275	8M12-class 10.9.
B1, B3	IPE 200 – S275	IPE 400 – S275	≠ 220×130×10 – S275	4M16-class 8.8.
B2	IPE 200 – S275	IPE 400 – S275	≠ 220×130×10 – S275	4M16-class 10.9.

2.2 Experimental testing

The experimental data have been collected during load application, with all results recorded during the complete loading program. Fig. 3 shows loading programs, the first contains several cycles of loading and unloading, while the second is a classical cyclic loading program. The benefits of the first loading program are presented in (Imamovic *et al*. 2015), where we elaborated that unloading points are essential for the potential existence of connection damage. Namely,

plasticity and damage models can represent the same behavior in the loading regime, but the unloading shows the difference between them. The first loading program has been used in four experimental tests, with only step size adjusted to the connection behavior, while the second loading program has been used in two tests.

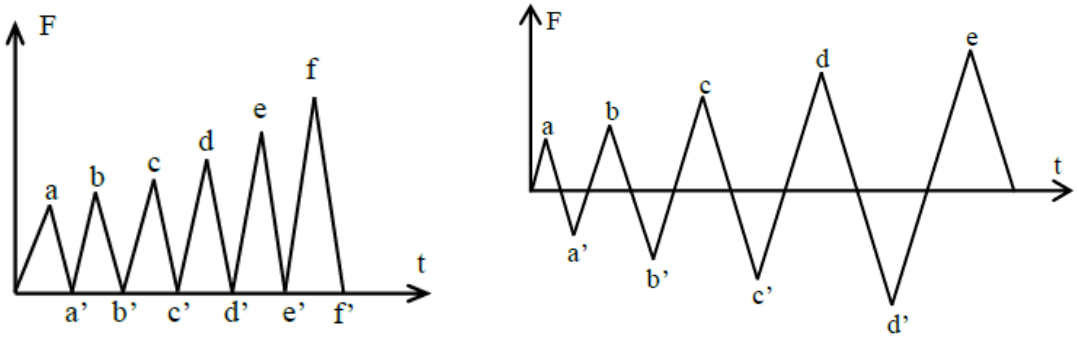

(a) Load applied in one direction (a) Cyclic load

Fig. 3 Loading programs

2.2.1 End plate connection with extended end plate

The end plate connection type with the extended plate is constructed from the plate (340×130×10 mm) welded to the vertical beam and eight bolts (M12) connecting the plate to the horizontal beam. The bolts were preloaded with 50% of pre-stressing force according to EC3. Two experimental tests have been performed for this connection type using the first loading program; the first test is denoted as A1 (bolt class 8.8.) and the second as A2 (bolt class 10.9.). The third experimental test A3 (experimental structure same as A1) has been conducted using the second loading program (cyclic loading).

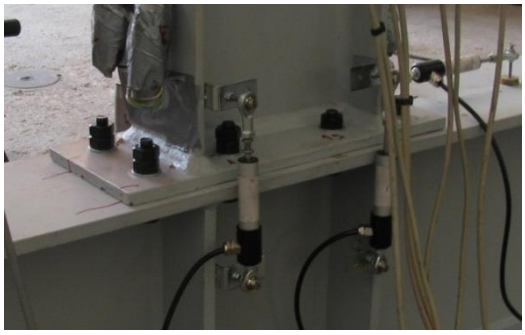

Fig. 4 End plate connection with extended end plate

The testing results are shown in Figs. 5-7, where we can see that vertical beam remains in the elastic response. The relative horizontal displacement between vertical and horizontal beam does not exist ($U_{2,Pi}^{\exp} = U_{S,Pi}^{\exp}$). In the first two tests (see Figs. 5 and 6) measured data shows that the

unloading lines at diagrams are parallel to first loading line, which indicates that plasticity model can represent the behavior of the connection.

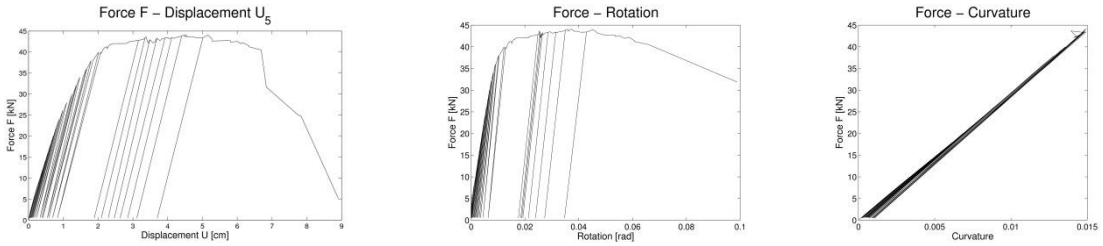

Fig. 5 Experimental results for connection A1

The measured responses under cyclic loading (see Fig. 7) indicate the complex behavior of the connection, which can not be presented by plasticity. This behavior is elaborated in next section, where we propose an appropriate constitutive model. The photographs in Fig. 8 show deformation of connection elements during experimental testing.

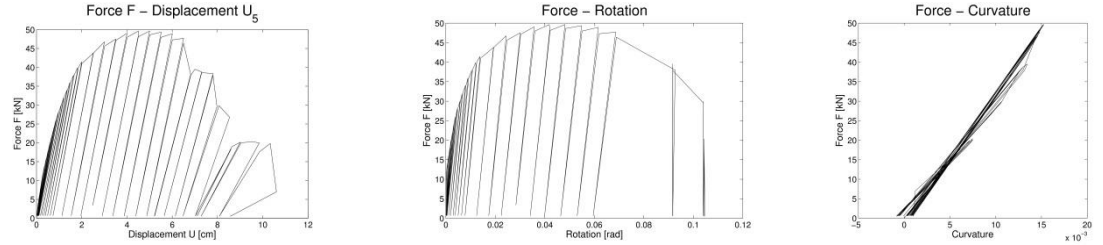

Fig. 6 Experimental results for connection A2

In first two experimental structures (A1 and A2), failure has progressively occurred in the bolts, where the inner row of bolts broke before the outer row of bolts. In the third test A3, displacement limit of measuring equipment was reached before the failure.

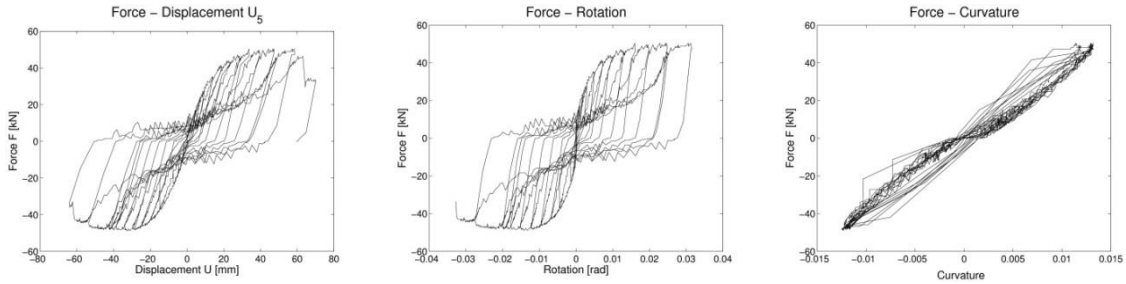

Fig. 7 Experimental results for connection A3

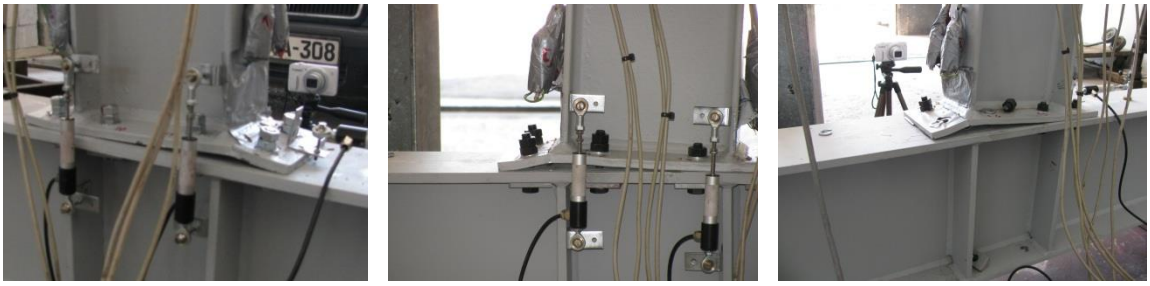

Fig. 8 Deformation of connection elements during experimental testing

2.2.2 End plate connection

The end plate connection (see Fig. 9) is constructed from the plate (220×130×10mm) welded to the vertical beam and four bolts (M16), connecting the plate to the horizontal beam. A total of three experimental tests have been conducted; two of them have done using the first loading program (B1 and B2) and one under cyclic loading (B3). The geometric characteristics and material quality of connection components are shown in Table 1.

Figs. 10 and 11 show testing results, where we can see that sliding displacement between vertical and horizontal beam has been measured. The strain gauges have not measured residual strains which indicate that vertical beam has remained in the linear elastic part of the response. The diagrams show that plasticity model can appropriately represent connection behavior because the subsequent loading/ unloading lines are parallel to the first loading line.

Fig. 9 End plate connection

The measured responses of the experimental structure B3 are shown in Fig. 12. By analyzing these responses, we can note the complex behavior of structural connection under cyclic load. Namely, after changing the direction of applied load, the less stiff response has been measured. In the next section, we propose model capable of representing measured responses.

In first two experimental structures (B1 and B2), failure has occurred in bolts, see Fig. 13. In the B1 test, both bolts in the tension zone broke at the same moment, while in the B2 experimental structure bolts gradually broke. Regarding the failure mechanism in the B1 test, where the brittle failure happened, we were not able to measure the softening response. In the third test B3, displacement limit of measuring equipment has been reached, so that failure has not bee occurred.

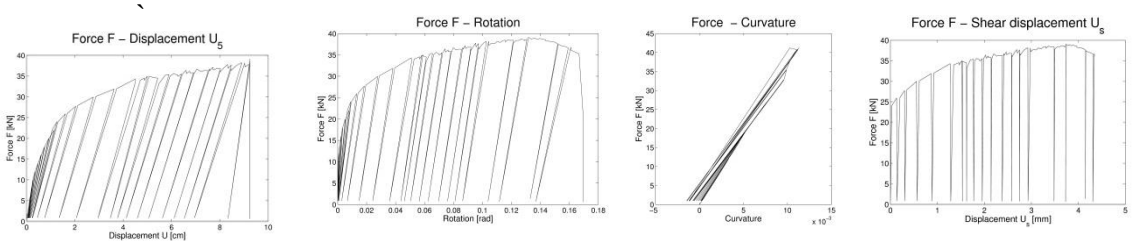

Fig. 10 Experimental results for connection B1

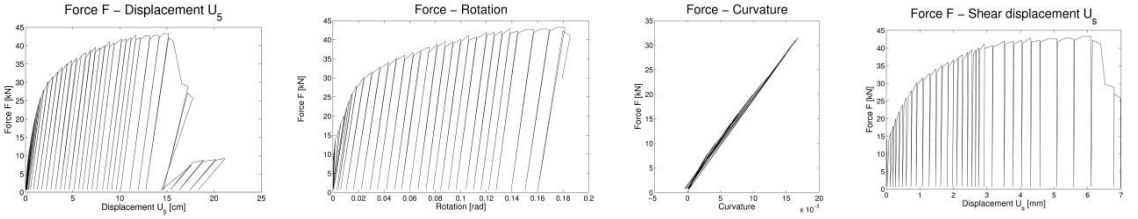

Fig. 11 Experimental results for connection B2

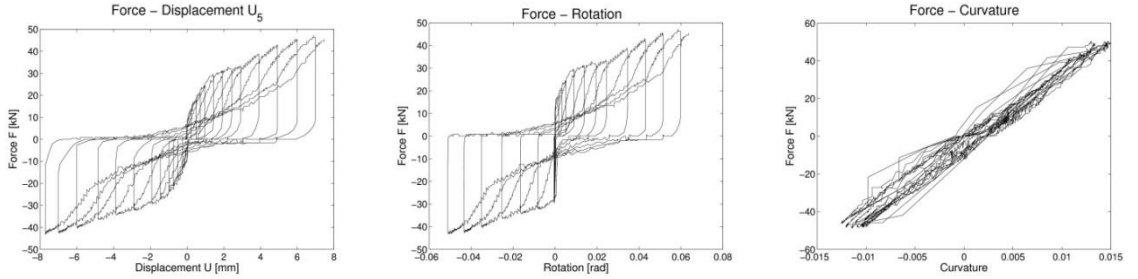

Fig. 12 Experimental results for connection B3

Fig. 13 Deformation of connection elements during experimental testing

2. Finite element beam model: Geometrically exact beam with bilinear hardening and nonlinear softening response

The experimental results show complex responses of tested structures, which are quite a challenge to describe. In this work, we propose the geometrically exact beam model (Imamovic *et al.* 2017) with hardening/softening response including modification related to the response under cyclic load. Namely, the large deformations of the connection components under cyclic loading

cause the less stiff response of the experimental structure. This phenomenon has a physical explanation. During the loading of the experimental structure, large deformations of the welded plate in the tension zone cause partial loss of the contact between the plate and horizontal beam, see Fig. 14(a). With the change in the direction of the applied load, the compression and tension zones will be inverted. The partially lost contact in compression zone causes the reduced stiffness of the connection, see Fig. 14(b). The stiffness remains reduced until the full contact between the plate and horizontal beam is reached again. After the full contact has been reached, the connection will provide again the full stiffness.

(a) (b)

Fig. 14 Deformation of the connection during a cyclic loading

This phenomenon can be captured with contact and solid elements in refined FEM models. Solid elements are able to represent large deformations and the nonlinear constitutive behavior. However, the refined FEM models are too complex for an everyday usage. For this reason, we propose the use of the beam element capable of representing the mentioned phenomenon.

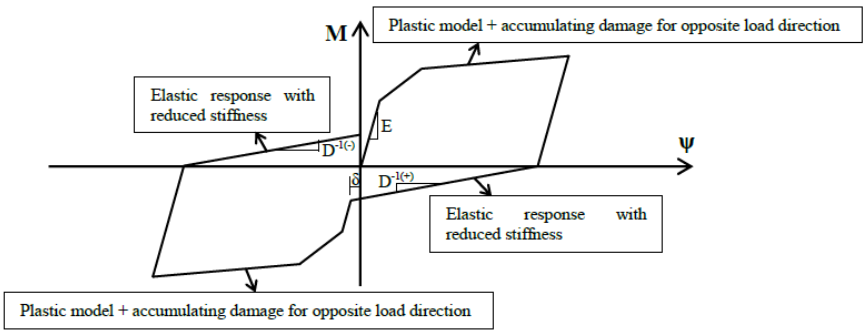

Fig. 15 Constitutive model

The idea is to use the coupled plasticity-damage model (Imamovic *et al*. 2015). The plasticity part governs the hardening and unloading phases, whereas the damage part provides the reduced stiffness of the connection after the change in the sign of the bending moment: from positive to negative or vice versa, see Fig. 15. The damage model governs connection response until full

contact between the plate and horizontal beam is reached. After the full contact has been reached, the plasticity model is again activated. The gap δ corresponds to the plastic deformation in bolts.

The constitutive model of the beam consists of bilinear hardening and linear softening (Imamovic *et al*. 2017). The hardening model is defined as coupled plasticity-damage model. The modification of the beam model requires splitting of internal variables into two groups, depending on the sign of bending moment. This model is capable of representing a previously described phenomenon which is commonly observed during experimental testing. A brief description of the beam's constitutive model is given as follows.

The Helmholtz free energy can be defined in a quadratic form, for both, a positive ($\bar{\Psi}^{(+)}$) and a negative ($\bar{\Psi}^{(-)}$) value of the bending moment (*M)*

$$\begin{aligned}
\bar{\Psi}^{(+)}(\bar{\mathbf{U}}^{e,(+)},\bar{\boldsymbol{\xi}}^{p,(+)},\bar{\mathbf{U}}^{d,(+)},\bar{\boldsymbol{\xi}}^{d,(+)}) &= \underbrace{\frac{1}{2}\bar{\mathbf{U}}^{e,T,(+)}\cdot\mathbf{C}^{(+)}\cdot\bar{\mathbf{U}}^{e,(+)}}_{\bar{\Psi}^{e,(+)}} + \underbrace{\frac{1}{2}\bar{\boldsymbol{\xi}}_1^{p,T,(+)}\cdot\mathbf{K}_1^{h,(+)}\cdot\bar{\boldsymbol{\xi}}_1^{p,(+)}}_{\bar{\Xi}_1^{p,(+)}} + \\
&+ \underbrace{\frac{1}{2}\bar{\boldsymbol{\xi}}_2^{p,T,(+)}\cdot\mathbf{K}_2^{h,(+)}\cdot\bar{\boldsymbol{\xi}}_2^{p,(+)}}_{\bar{\Xi}_2^{p,(+)}} + \underbrace{\mathbf{T}\bar{\mathbf{U}}^{d,(+)} - \frac{1}{2}\mathbf{T}D^{(+)}\mathbf{T}}_{\bar{\Psi}^{d,(+)}} + \underbrace{\frac{1}{2}\bar{\xi}^{d,(+)}\bar{K}^{d,(+)}\bar{\xi}^{d,(+)}}_{\bar{\Xi}^{d,(+)}} \\
\bar{\Psi}^{(-)}(\bar{\mathbf{U}}^{e,(-)},\bar{\boldsymbol{\xi}}^{p,(-)},\bar{\mathbf{U}}^{d,(-)},\bar{\boldsymbol{\xi}}^{d,(-)}) &= \underbrace{\frac{1}{2}\bar{\mathbf{U}}^{e,T,(-)}\cdot\mathbf{C}^{(-)}\cdot\bar{\mathbf{U}}^{e,(-)}}_{\bar{\Psi}^{e,(-)}} + \underbrace{\frac{1}{2}\bar{\boldsymbol{\xi}}_1^{p,T,(-)}\cdot\mathbf{K}_1^{h,(-)}\cdot\bar{\boldsymbol{\xi}}_1^{p,(-)}}_{\bar{\Xi}_1^{p,(-)}} + \\
&+ \underbrace{\frac{1}{2}\bar{\boldsymbol{\xi}}_2^{p,T,(-)}\cdot\mathbf{K}_2^{h,(-)}\cdot\bar{\boldsymbol{\xi}}_2^{p,(-)}}_{\bar{\Xi}_2^{p,(-)}} + \underbrace{\mathbf{T}\bar{\mathbf{U}}^{d,(-)} - \frac{1}{2}\mathbf{T}D^{(-)}\mathbf{T}}_{\bar{\Psi}^{d,(-)}} + \underbrace{\frac{1}{2}\bar{\xi}^{d,(-)}\bar{K}^{d,(-)}\bar{\xi}^{d,(-)}}_{\bar{\Xi}^{d,(-)}}
\end{aligned} \tag{3}$$

where: $\bar{\mathbf{U}}^e, \bar{\mathbf{U}}^d$ are elastic and damage strain measure tensors; $\bar{\boldsymbol{\xi}}_i^p, \bar{\boldsymbol{\xi}}_i^d$ are vectors of hardening variables of the plastic and damage model, respectively; *D* is the internal damage variable; $\mathbf{K}_i^h, \mathbf{K}^d$ are the corresponding hardening moduli of the plastic and damage model; and **T** is Biot's stress tensor. Every symbol contains two symbols. The first corresponds to the positive $(\bullet^{(+)})$, and the second to the negative $(\bullet^{(-)})$ bending moment. The yield criterion, defined as multi-criteria (plasticity and damage), can be completely different for the positive and the negative bending moment. However, in this work we have assumed that the response in the hardening regime is symmetric

$$\begin{aligned}
\bar{\phi}_i^p(T_i,\bar{q}_i^p) &\le 0 \\
\bar{\phi}_i^d(T_i,\bar{q}_i^d) &\le 0
\end{aligned} \tag{4}$$

where $\bar{\mathbf{q}}$ is the vector of internal hardening stress like variables. The second principle of thermodynamics states that the plastic dissipation must remain non-negative

$$\begin{aligned}
0 \le \bar{\mathcal{D}} = \underbrace{\dot{\bar{\mathbf{T}}}\left(\frac{\partial\bar{\chi}^e}{\partial\mathbf{T}} - \bar{\mathbf{U}}^e\right) + \dot{\bar{\mathbf{T}}}\left(\frac{\partial\bar{\chi}^d}{\partial\mathbf{T}} - \bar{\mathbf{U}}^d\right)}_{\bar{\mathcal{D}}^e=0} + \underbrace{\mathbf{T}\dot{\bar{\mathbf{U}}}_1^p - \frac{\partial\bar{\boldsymbol{\Xi}}_1^p}{\partial\bar{\boldsymbol{\xi}}_1^p}\frac{d\bar{\boldsymbol{\xi}}_1^p}{dt}}_{\bar{\mathcal{D}}_1^p} + \\
+ \underbrace{\mathbf{T}\dot{\bar{\mathbf{U}}}_2^p - \frac{\partial\bar{\boldsymbol{\Xi}}_2^p}{\partial\bar{\boldsymbol{\xi}}_2^p}\frac{d\bar{\boldsymbol{\xi}}_2^p}{dt}}_{\bar{\mathcal{D}}_2^p} + \underbrace{\frac{\partial\bar{\mathbf{U}}^d}{\partial\bar{D}}\dot{\bar{D}} - \frac{\partial\bar{\Xi}^d}{\partial\bar{\xi}^d}\dot{\bar{\xi}}^d}_{\bar{\mathcal{D}}^d}
\end{aligned} \tag{5}$$

where $\bar{\chi}$ is complementary energy, see (Ibrahimbegovic 2009). The principle of maximum

plastic dissipation can be formulated (Hill 1950, Ibrahimbegovic and Frey 1993a) as the minimization problem with the constraint, with the latter being yield function (4). This can further be recast as a corresponding unconstrained minimization by using the Lagrange multiplier method

$$\min_{\mathbf{T},\bar{\mathbf{q}}} \max_{\dot{\bar{\gamma}}} \left[\bar{L}^p(\mathbf{T},\bar{\mathbf{q}}^p,\dot{\bar{\boldsymbol{\gamma}}}^p) = -\bar{\mathcal{D}}^p(\mathbf{T},\bar{\mathbf{q}}^p) + \dot{\bar{\gamma}}_i^p \cdot \bar{\phi}_i^p(\mathbf{T},\bar{\mathbf{q}}^p) \right] \tag{6}$$

where $\dot{\bar{\gamma}}_i^p$ are Lagrange multipliers of the plasticity. The Kuhn-Tucker optimality conditions provide the evolution equations for internal variables in rate form along with the loading/unloading conditions

$$\begin{aligned} &\frac{\partial \bar{L}_i^p}{\partial \mathbf{T}} = -\dot{\bar{\mathbf{U}}}_i^p + \dot{\bar{\gamma}}_i^p \frac{\partial \bar{\phi}_i^p}{\partial \mathbf{T}} = 0 \Rightarrow \dot{\bar{\mathbf{U}}}_i^p = \dot{\bar{\gamma}}_i^p \frac{\partial \bar{\phi}_i^p}{\partial \mathbf{T}} \\ &\frac{\partial \bar{L}_i^p}{\partial \bar{\mathbf{q}}_i} = -\frac{\partial \bar{\xi}_i^p}{\partial t} + \dot{\bar{\gamma}}_i^p \frac{\partial \bar{\phi}_i^p}{\partial \bar{\mathbf{q}}_i^p} = 0 \Rightarrow \frac{\partial \bar{\xi}_i^p}{\partial t} = \dot{\bar{\gamma}}_i^p \frac{\partial \bar{\phi}_i^p}{\partial \bar{\mathbf{q}}_i^p} \\ &\dot{\bar{\gamma}}_i^p \geq 0, \quad \bar{\phi}_i^p \leq 0, \quad \dot{\bar{\gamma}}_i^p \bar{\phi}_i^p = 0 \end{aligned} \tag{7}$$

The appropriate value of plastic multiplier $\dot{\bar{\boldsymbol{\gamma}}}^p$ can be determined from the plastic consistency condition for the case of sustained plastic flow

$$\dot{\bar{\phi}}_i^p = 0 \;\Rightarrow\; \dot{\bar{\gamma}}_i^p = \frac{\dfrac{\partial \bar{\phi}_i^p}{\partial \mathbf{T}} \mathbf{C}^e \dot{\bar{\mathbf{U}}}}{\dfrac{\partial \bar{\phi}_i^p}{\partial \mathbf{T}} \mathbf{C}^e \dfrac{\partial \bar{\phi}_i^p}{\partial \mathbf{T}} + \dfrac{\partial \bar{\phi}_i^p}{\partial \bar{\mathbf{q}}_i^p} \mathbf{K}_i^h \dfrac{\partial \bar{\phi}_i^p}{\partial \bar{\mathbf{q}}_i^p}} \tag{8}$$

By replacing the last result in stress rate equation, we can obtain the elastoplastic modulus $\mathbf{C}^{ep}$ that should replace the elastic modulus $\mathbf{C}$ in the plastic regime

$$C_i^{ep} = \mathbf{C}^e - \frac{\mathbf{C}^e \dfrac{\partial \bar{\phi}_i^p}{\partial \mathbf{T}} \otimes \mathbf{C}^e \dfrac{\partial \bar{\phi}_i^p}{\partial \mathbf{T}}}{\dfrac{\partial \bar{\phi}_i^p}{\partial \mathbf{T}} \mathbf{C}^e \dfrac{\partial \bar{\phi}_i^p}{\partial \mathbf{T}} + \dfrac{\partial \bar{\phi}_i^p}{\partial \bar{\mathbf{q}}_i^p} \mathbf{K}_i^h \dfrac{\partial \bar{\phi}_i^p}{\partial \bar{\mathbf{q}}_i^p}} \tag{9}$$

The principle of maximum damage dissipation states that among all the variables $(T_i, \bar{q}_i^d)$ that satisfy the damage yield criterion $\bar{\phi}_i^d\left(T_i, \bar{q}_i^d\right)$, we have to select those that maximize damage dissipation. This can be written as a constrained minimization problem

$$\min_{\mathbf{T},\bar{\mathbf{q}}} \max_{\dot{\bar{\gamma}}} \left[\bar{L}^d(\mathbf{T},\bar{\mathbf{q}}^d,\dot{\bar{\boldsymbol{\gamma}}}^d) = -\bar{\mathcal{D}}^d(\mathbf{T},\bar{\mathbf{q}}^d) + \dot{\bar{\gamma}}_i^d \cdot \bar{\phi}_i^d(\mathbf{T},\bar{\mathbf{q}}^d) \right] \tag{10}$$

where the damage multiplier $\dot{\bar{\gamma}}^d \geq 0$ plays the role of Lagrange multiplier. By appealing to the Kuhn-Tucker optimality conditions, from the last result, we can obtain the evolution equations for internal variables along with the loading/unloading conditions

$$\begin{aligned}
&\frac{\partial \bar{L}_i^d}{\partial \mathbf{T}} = -\dot{\bar{\mathbf{U}}}_i^d + \dot{\bar{\gamma}}_i^d \frac{\partial \bar{\phi}_i^d}{\partial \mathbf{T}} = 0 \Rightarrow \dot{\bar{\mathbf{U}}}_i^d = \dot{\bar{\gamma}}_i^d \frac{\partial \bar{\phi}_i^d}{\partial \mathbf{T}} \\
&\frac{\partial \bar{L}_i^d}{\partial \bar{\mathbf{q}}_i^d} = -\frac{\partial \bar{\xi}_i^d}{\partial t} + \dot{\bar{\gamma}}_i^d \frac{\partial \bar{\phi}_i^d}{\partial \bar{\mathbf{q}}_i^d} = 0 \Rightarrow \frac{\partial \bar{\xi}_i^d}{\partial t} = \dot{\bar{\gamma}}_i^d \frac{\partial \bar{\phi}_i^d}{\partial \bar{\mathbf{q}}_i^d} \\
&\dot{\bar{\gamma}}_i^d \geq 0, \;\; \bar{\phi}_i^d \leq 0, \;\; \dot{\bar{\gamma}}_i^d \bar{\phi}_i^d = 0
\end{aligned} \tag{11}$$

The appropriate value of the plastic multiplier $\dot{\bar{\gamma}}^p$ can be determined from the damage consistency condition for the case of sustained damage flow

$$\dot{\bar{\phi}}_i^p = 0 \;\Rightarrow\; \dot{\bar{\gamma}}_i^p = \frac{\dfrac{\partial \bar{\phi}_i^p}{\partial \mathbf{T}} \mathbf{C}^e \dot{\bar{\mathbf{U}}}}{\dfrac{\partial \bar{\phi}_i^p}{\partial \mathbf{T}} \mathbf{C}^e \dfrac{\partial \bar{\phi}_i^p}{\partial \mathbf{T}} + \dfrac{\partial \bar{\phi}_i^p}{\partial \bar{\mathbf{q}}_i^p} \mathbf{K}_i^h \dfrac{\partial \bar{\phi}_i^p}{\partial \bar{\mathbf{q}}_i^p}} \tag{12}$$

By replacing the last result in the stress rate equation, we can obtain the damage modulus $\mathbf{C}^{ed}$ that should replace the elastic modulus $\mathbf{C}$ in the damage regime

$$C_i^{ed} = \mathbf{C}^e - \frac{\mathbf{C}^e \dfrac{\partial \bar{\phi}_i^d}{\partial \mathbf{T}} \otimes \mathbf{C}^e \dfrac{\partial \bar{\phi}_i^d}{\partial \mathbf{T}}}{\dfrac{\partial \bar{\phi}_i^d}{\partial \mathbf{T}} \mathbf{C}^e \dfrac{\partial \bar{\phi}_i^d}{\partial \mathbf{T}} + \dfrac{\partial \bar{\phi}_i^d}{\partial \bar{\mathbf{q}}_i^d} \mathbf{K}_i^d \dfrac{\partial \bar{\phi}_i^d}{\partial \bar{\mathbf{q}}_i^d}} \tag{13}$$

The Eqs. (6)-(13) should be separately written for positive and negative value of the bending moment, but in order to save space, we have expressed them independently of the sign.

We note in passing that the elastoplastic tangent above remains the same in the discrete problem, obtained by using the backward Euler time integration scheme.

In the softening regime, for the both the positive and the negative value of the bending moment, the Helmholtz free energy can be written in a quadratic form in terms of softening variables

$$\begin{aligned}
&\bar{\bar{\Psi}}^{(+)}\left(\bar{\bar{\boldsymbol{\xi}}}^{s,(+)}\right) = \underbrace{\frac{1}{2} \bar{\bar{\boldsymbol{\xi}}}^{s,(+)} \mathbf{K}_s^{(+)} \bar{\bar{\boldsymbol{\xi}}}^{s,(+)}}_{\bar{\Xi}^{s,(+)}}; \;\; \Psi^{(+)}(\cdot) = \bar{\Psi}^{(+)}(\cdot) + \bar{\bar{\Psi}}^{(+)}(\bar{\bar{\boldsymbol{\xi}}}^{s,(+)}) \delta_{\bar{x}} \\
&\bar{\bar{\Psi}}^{(-)}\left(\bar{\bar{\boldsymbol{\xi}}}^{s,(-)}\right) = \underbrace{\frac{1}{2} \bar{\bar{\boldsymbol{\xi}}}^{s,(-)} \mathbf{K}_s^{(-)} \bar{\bar{\boldsymbol{\xi}}}^{s,(-)}}_{\bar{\Xi}^{s,(-)}}; \;\; \Psi^{(-)}(\cdot) = \bar{\Psi}^{(-)}(\cdot) + \bar{\bar{\Psi}}^{(-)}(\bar{\bar{\boldsymbol{\xi}}}^{s,(-)}) \delta_{\bar{x}}
\end{aligned} \tag{14}$$

where $\bar{\bar{\boldsymbol{\xi}}}^s$ is a set of internal variables representing the connection failure and $\bar{\bar{\mathbf{K}}}^s$ is a set of the softening moduli. The yield function for softening is chosen in a multi-criteria form pertaining to bending, shearing, and axial force

$$\begin{aligned}
&\text{Positive value of } M\text{: } \dot{\bar{\bar{\gamma}}}_i^{(+)} \bar{\bar{\phi}}_i^{(+)} = 0 \Rightarrow \bar{\bar{\phi}}_i^{(+)}(t_i^{(+)}, \bar{\bar{q}}_i^{s,(+)}) \leq 0 \\
&\text{Negative value of } M\text{: } \dot{\bar{\bar{\gamma}}}_i^{(-)} \bar{\bar{\phi}}_i^{(-)} = 0 \Rightarrow \bar{\bar{\phi}}_i^{(-)}(t_i^{(-)}, \bar{\bar{q}}_i^{s,(-)}) \leq 0
\end{aligned} \tag{15}$$

where $t_i^{(+)}, t_i^{(-)}$ are traction forces and $\bar{\bar{q}}_i^{s,(+)}, \bar{\bar{q}}_i^{s,(-)}$ are stress-like variables work-conjugate to softening variables at the discontinuity for the corresponding failure mode. The principal of

maximum dissipation (Hill 1950) among all admissible values of these variables, will pick the ones that maximize the softening dissipation. This can be solved as an unconstrained minimization problem. The result is the evolution equations for internal variables along with the loading/unloading conditions

$$\begin{aligned}&\frac{\partial \bar{\bar{L}}^s}{\partial \bar{\bar{\mathbf{q}}}^s}=-\dot{\bar{\bar{\xi}}}^s+\sum\nolimits_1^3 \dot{\bar{\bar{\gamma}}}\frac{\partial \bar{\bar{\phi}}}{\partial \bar{\bar{\mathbf{q}}}^s}=0 \Rightarrow \dot{\bar{\bar{\xi}}}^s=\sum\nolimits_1^3 \dot{\bar{\bar{\gamma}}}_i\frac{\partial \bar{\bar{\phi}}}{\partial \bar{\bar{\mathbf{q}}}^s}\\&\dot{\bar{\bar{\gamma}}}\geq 0,\ \ \bar{\bar{\phi}}\leq 0,\ \ \dot{\bar{\bar{\gamma}}}\bar{\bar{\phi}}=0\end{aligned} \tag{16}$$

The last Eq. (16) can be separately written for the positive and the negative values of the bending moment.

The beam kinematics equations can be written by using the rotated strain measure: $\mathbf{H}=\mathbf{U}-\mathbf{I}$, where the only non-zero components are defined as

$$H_{11}=\Sigma-\zeta K,\ H_{21}=\Gamma \tag{17}$$

The explicit form of generalized strains can be written as

$$\begin{aligned}\Sigma=H_{11}^{u,v}&=\underbrace{\left(1+\frac{d\bar{u}}{dx}\right)\cos\psi+\frac{d\bar{v}}{dx}\sin\psi-1}_{\bar{\Sigma}}+\underbrace{\left(\frac{d\bar{\bar{u}}}{dx}\cos\psi+\frac{d\bar{\bar{v}}}{dx}\sin\psi\right)}_{\bar{\bar{\Sigma}}}\delta_{\bar{x}}\\ \Gamma=H_{21}^{u,v}&=\underbrace{-\left(1+\frac{d\bar{u}}{dx}\right)\sin\psi+\frac{d\bar{v}}{dx}\cos\psi}_{\bar{\Gamma}}+\underbrace{\left(-\frac{d\bar{\bar{u}}}{dx}\sin\psi+\frac{d\bar{\bar{v}}}{dx}\cos\psi\right)}_{\bar{\bar{\Gamma}}}\delta_{\bar{x}}\\ K=H_{11}^{\psi}&=\underbrace{\frac{d\bar{\psi}}{dx}}_{\bar{K}}+\underbrace{\frac{d\bar{\bar{\psi}}}{dx}}_{\bar{\bar{K}}}\delta_{\bar{x}}\end{aligned} \tag{18}$$

By using the same notation for the virtual strains (denoted with superposed $(\hat{\bullet})$), we can write the weak form of equilibrium equation, see (Ibrahimbegovic and Frey 1993a)

$$G(\mathbf{a},\hat{\mathbf{a}}):=\int_L\left(\hat{\Sigma}N+\hat{\Gamma}V+\hat{K}M\right)dx-G^{ext}(\hat{\mathbf{a}})=0 \tag{19}$$

In (19) above, N, V, and M denote stress resultants regarding the Biot stress

$$\boldsymbol{\sigma}=(N,V,M)^T;\ \ N=\int_A T^{11}dA;\ \ V=\int_A T^{21}dA;\ M=-\int_A \zeta T^{11}dA \tag{20}$$

The yield function for the hardening is chosen in a multi-criteria form pertaining to the bending moment, shear and axial force, respectively

$$\begin{aligned}&\dot{\bar{\gamma}}_i^p\bar{\phi}_i^p=0\Rightarrow\begin{bmatrix}\bar{\phi}_M^p(M,\bar{q}_M^p)=|M|-\left(M_y-\bar{q}_M^p\right)\leq 0\\ \bar{\phi}_V^p(V,\bar{q}_V^p)=|V|-\left(V_y-\bar{q}_V^p\right)\leq 0\\ \bar{\phi}_N^p(N,\bar{q}_N^p)=|N|-\left(N_y-\bar{q}_N^p\right)\leq 0\end{bmatrix}\\&\dot{\bar{\gamma}}_i^d\bar{\phi}_i^d=0\Rightarrow\bar{\phi}_M^d(M,\bar{q}_M^d)=|M|-\left(M_f-\bar{q}_M^d\right)\leq 0\end{aligned} \tag{21}$$

Table 2 Computational procedure for a characteristic iteration

Given: $\Delta K_n^{(i)} = K_{n+1}^{(i)} - K_n^{(i)}, K_n^{p,(+)}, D_n^{(-)}, \xi_n^{p,(+)}, K_n^{p,(-)}, D_n^{(+)}, \xi_n^{p,(-)}, M_n$

Find: $M_{n+1}, K_{n+1}^{p(i),(+)}, D_{n+1}^{(i),(-)}, \xi_{n+1}^{p(i),(+)}, K_{n+1}^{p(i),(-)}, D_{n+1}^{(i),(+)}, \xi_{n+1}^{p(i),(-)}$

IF($M_n \geq 0$ and $K_{n+1}^{(i)} \geq \left|\delta^{(-)}\right|$ and 'damage=false')

Elastic trial step => $M_{n+1}^{trial} = M_n + EI\left(\Delta K_{n+1}^{(i)} - K_n^{p,(+)}\right)$ => damage = false

Plasticity	*Damage*
$\bar{\phi}_{M,n+1}^{p,trial}(M, \bar{q}_M^{p,(+)}) = \left\|M_{n+1}^{trial}\right\| - \left(M_y - \bar{q}_{M,n}^{p,(+)}\right)$	$\bar{\phi}_{M,n+1}^{d,trial}(M, \bar{q}_M^{d,(+)}) = \left\|M_{n+1}^{trial}\right\| - \left(M_f - \bar{q}_{M,n}^{d,(+)}\right)$
IF $\bar{\phi}_{M,n+1}^{p,trial}(M, \bar{q}_M^{p,(+)}) \leq 0$	*IF* $\bar{\phi}_{M,n+1}^{d,trial}(M, \bar{q}_M^{d,(+)}) \leq 0$
$M_{n+1}^{p} = M_{n+1}^{trial}; K_{n+1}^{p,(+)} = K_n^{p,(+)}; \xi_{n+1}^{p,(+)} = \xi_n^{p,(+)}$	$M_{n+1}^{d} = M_{n+1}^{trial}; D_{n+1}^{(+)} = D_n^{(+)}; \xi_{n+1}^{d,(+)} = \xi_n^{d,(+)}$
ELSEIF $\bar{\phi}_{M,n+1}^{p,trial}(M, \bar{q}_M^{p,(+)}) > 0$	*ELSEIF* $\bar{\phi}_{M,n+1}^{d,trial}(M, \bar{q}_M^{d,(+)}) > 0$
solve $\bar{\phi}_{M,n+1}^{p}(M, \bar{q}_M^{p,(+)}) = 0$ *with*	*solve* $\bar{\phi}_{M,n+1}^{d}(M, \bar{q}_M^{d,(+)}) = 0$ *with*
$M_{n+1} = M_{n+1}^{trial} - \gamma_{n+1}^{p} EI \dfrac{\partial \bar{\phi}_{M,n+1}^{p}}{\partial M}$	$M_{n+1}^{d} = M_{n+1}^{trial} - \gamma_{n+1}^{d} D_n^{-1,(+)} \dfrac{\partial \phi_{M,n+1}^{d}}{\partial M}$
$K_{n+1}^{p,(+)} = K_n^{p,(+)} + \gamma_{n+1}^{p} \dfrac{\partial \bar{\phi}_{M,n+1}^{p}}{\partial M}$	$D_{n+1}^{(+)} = D_n^{(+)} + \gamma_{n+1}^{d} \dfrac{1}{\left\|M_{n+1}^{d}\right\|}$
$\xi_{n+1}^{p,(+)} = \xi_n^{p,(+)} + \gamma_{n+1}^{p}$	$(\delta^{(+)} =) \xi_{n+1}^{d,(+)} = \xi_n^{d,(+)} + \gamma_{n+1}^{d}$

ELSEIF($\dfrac{M_{n+1}^{trial}}{M_n} < 0$ and $K_{n+1}^{(i)} \geq -\left|\delta^{(+)}\right|$) or *ELSEIF*($M_n < 0$ and 'damage=true')

Elastic step with reduced stiffness

$M_{n+1}^{trial} = M_n + D_n^{-1,(+)} I\left(\Delta K_{n+1}^{(i)} - K_n^{p,(+)}\right)$ => damage = true

$M_{n+1} = M_{n+1}^{trial}; K_{n+1}^{p,(+)} = K_n^{p,(+)}; \xi_{n+1}^{p,(+)} = \xi_n^{p,(+)}$

ELSEIF($\dfrac{M_{n+1}^{trial}}{M_n} > 0$ and $K_{n+1}^{(i)} < -\left|\delta^{(+)}\right|$) or *ELSEIF*($M_n < 0$ and 'damage=false')

Elastic trial step

$M_{n+1}^{trial} = M_n + EI\left(\Delta K_{n+1}^{(i)} - K_n^{p,(-)}\right)$ => *damage = false*

Plasticity	*Damage*
$\bar{\phi}_{M,n+1}^{p,trial}(M, \bar{q}_M^{p,(-)}) = \left\|M_{n+1}^{trial}\right\| - \left(M_y - \bar{q}_{M,n}^{p,(-)}\right)$	$\bar{\phi}_{M,n+1}^{d,trial}(M, \bar{q}_M^{d,(-)}) = \left\|M_{n+1}^{trial}\right\| - \left(M_f - \bar{q}_{M,n}^{d,(-)}\right)$
IF $\bar{\phi}_{M,n+1}^{p,trial}(M, \bar{q}_M^{p,(-)}) \leq 0$	*IF* $\bar{\phi}_{M,n+1}^{d,trial}(M, \bar{q}_M^{d,(-)}) \leq 0$
$M_{n+1}^{p} = M_{n+1}^{trial}; K_{n+1}^{p} = K_n^{p}; \xi_{n+1}^{p} = \xi_n^{p}$	$M_{n+1}^{d} = M_{n+1}^{trial}; D_{n+1} = D_n; \xi_{n+1}^{d} = \xi_n^{d}$
ELSEIF $\bar{\phi}_{M,n+1}^{p,trial}(M, \bar{q}_M^{p,(-)}) > 0$	*ELSEIF* $\bar{\phi}_{M,n+1}^{d,trial}(M, \bar{q}_M^{d,(+)}) > 0$
solve $\bar{\phi}_{M,n+1}^{p}(M, \bar{q}_M^{p,(-)}) = 0$ *with*	*solve* $\bar{\phi}_{M,n+1}^{d}(M, \bar{q}_M^{d,(+)}) = 0$ *with*
$M_{n+1} = M_{n+1}^{trial} - \gamma_{n+1}^{p} EI \dfrac{\partial \bar{\phi}_{M,n+1}^{p}}{\partial M}$	$M_{n+1}^{d} = M_{n+1}^{trial} - \gamma_{n+1}^{d} D_n^{-1} \dfrac{\partial \phi_{M,n+1}^{d}}{\partial M}$
$K_{n+1}^{p,(-)} = K_n^{p,(-)} + \gamma_{n+1}^{p} \dfrac{\partial \bar{\phi}_{M,n+1}^{p}}{\partial M}$	$D_{n+1}^{(-)} = D_n^{(-)} + \gamma_{n+1}^{d} \dfrac{1}{\left\|M_{n+1}^{d}\right\|}$
$\xi_{n+1}^{p,(-)} = \xi_n^{p,(-)} + \gamma_{n+1}^{p}$	$\left(\delta^{(-)} =\right) \xi_{n+1}^{d,(-)} = \xi_n^{d,(-)} + \gamma_{n+1}^{d}$

Table 2 Continued

$ELSEIF(\frac{M_{n+1}^{trial}}{M_n}<0$ and $K_{n+1}^{(i)}<\left\|\delta^{(-)}\right\|)$ or $ELSEIF(M_n>0$ and 'damage=true')
Elastic step with reduced stiffness
$M_{n+1}^{trial}=M_n+D_n^{-1,(-)}I\left(\Delta K_{n+1}^{(i)}-K_n^{p,(-)}\right)$ => damage=true $M_{n+1}=M_{n+1}^{trial};K_{n+1}^{p,(-)}=K_n^{p,(-)};\xi_{n+1}^{p,(-)}=\xi_n^{p,(-)}$

where M is the bending moment; V is the shear force; N is the axial force; $\bar{q}_M^p$, $\bar{q}_V^p$, $\bar{q}_N^p$ and $\bar{q}_M^d$ are internal hardening stress like variables($\bullet^p$ - plasticity; $\bullet^d$ - damage model); whereas M_y, V_y and N_y denote yield the bending moment, shear force and axial force, while M_f denotes bending moment at the beginning of the damage flow. The internal variable q_M^p provides bilinear hardening related to the bending moment, which can be written as

$$q_M^p=\begin{cases}-K_{M,1}^h\bar{\xi}_M^p;\ 0\le\bar{\xi}_M^p<\bar{\xi}_{M_y}^p\\-K_{M,2}^h\bar{\xi}_M^p;\ \bar{\xi}_{M_y}^p\le\bar{\xi}_M^p<\infty\end{cases} \tag{22}$$

where $K_{M,1}^h$ and $K_{M,2}^h$ are the hardening moduli. The Eqs. (16)-(22) should be separately written for the positive and negative value of the bending moment, but they are expressed in a form independent on the sign.

At the end of this section, we present the computational procedure (Table 2) for a characteristic iteration. This procedure presents the local phase for computing the value of the bending moment. Other internal force can be computed in the same way.

4. Identification of the constitutive model parameters

In the case of a structural connection testing, the global response of a specimen can be represented with load-displacement (F-u) diagram. Any such curve can be related to the three phases of the connection response: elastic, hardening and softening part. The used damage-plasticity model, which represents connection behavior, contains the bilinear hardening and the linear softening response. For the most general case, we need to identify three parameters in the elastic phase, nine in the hardening phase and six unknown parameters in the softening phase.

The identification in general case is performed in two steps: i) definition of an objective function based on some experimental measurements; ii) minimization of this objective function in order to find values of constitutive parameters used in the model.

The choice of the objective function is a crucial step to ensure the success of the minimization. In general case, the objective function can be defined as the gap between measured and computed response values (displacement, stress, deformation, reaction force, etc.)

$$J(\mathbf{d}_\mathrm{p})=\sum_{j\in J}n\left(\mathbf{u}_j^{com}(\mathbf{d}_\mathrm{p})-\mathbf{u}_j^{\exp}\right)^2 \tag{23}$$

where $\mathbf{d}_\mathrm{p}$ are the model parameters that we seek to identify, $\mathbf{u}_j^{com}(\mathbf{d}_\mathrm{p})$ and $\mathbf{u}_j^{\exp}$ are, respectively,

computed and experimentally measured values of displacements/stresses/strains, and n is the weighting factor for different terms of objective function.

Minimization of the objective function can formally be written as minimization under constraint

$$\min_{G(\sigma;\delta w)=0} J(\mathbf{d}_{\mathrm{p}}) = \sum_{j\in J} n\left(\mathbf{u}_j^{com}(\mathbf{d}_{\mathrm{p}}) - \mathbf{u}_j^{\exp}\right)^2 \tag{24}$$

where the weak form of equilibrium equations $G(\varepsilon,\zeta^p,\zeta^d;\delta w)=0$ is the corresponding constraint. Namely, the weak form of equilibrium equations has to be satisfied at every time step. The constrained minimization of the objective function can be transferred into unconstrained minimization by using the Lagrange multiplier method (Ibrahimbegovic *et al.* 2004)

$$\max_{\forall\lambda}\ \min_{G(\sigma;\mathbf{d}_p)=0} L(\sigma,\mathbf{d}_{\mathrm{p}},\lambda) = J(\mathbf{d}_p) + \mathrm{G}(\sigma,\mathbf{d}_{\mathrm{p}},\lambda) \tag{25}$$

where λ are Lagrange multipliers inserted into the weak form of equilibrium equations instead of virtual displacements. This type of minimization of the objective function is very complex for seventeen unknown parameters. However, if we split an unconstrained minimization of the objective function into several phases, then we will decrease the number of unknown to maximal of two parameters in each phase (Kucerova *et al*. 2009).

The general identification procedure of the connection model parameters is presented in the flowchart in Fig. 16. The process is split into three phases, with every phase further split into few cases. The first phase seeks to identify the three constitutive parameters related to elastic response: S_{jb}^{in} - initial rotational stiffness, S_{js}^{in} - initial shearing stiffness and S_{ja}^{in} - initial axial stiffness. The second phase deals with nine unknown parameters related to hardening plasticity: V_y^{con} - yield shear force; S_{js}^{p} - hardening stiffness modulus with respect to shear force; N_y^{con} - yield axial force; S_{ja}^{p} - hardening stiffness modulus with respect to axial force; $M_{y,1}^{con}$ - first yield bending moment; $S_{jb,1}^{p}$ - first hardening stiffness modulus with respect to bending moment; $M_{y,2}^{con}$ - second yield bending moment; $S_{jb,2}^{p}$ - the second hardening stiffness modulus with respect to bending moment; S_{jb}^{d} - the hardening stiffness modulus with respect to bending moment and damage model . The last phase deals with six softening constitutive parameters: N_u^{con} - ultimate axial force, S_{ja}^{s} - the softening modulus with respect to axial force, V_u^{con} - ultimate shear force, S_{js}^{s} - softening stiffness modulus with respect to shear force, M_u^{con} - ultimate bending moment and S_{jb}^{s} - softening modulus with respect to bending moment.

The stiffnesses can be obtained from the identified constitutive parameters of the proposed beam, as follows

$$S_{jb}^{in}=\frac{EI}{L};\ S_{jb,i}^{p}=\frac{K_{M,1}^{h}I}{L};\ S_{jb}^{d}=\frac{K_M^d I}{L};\ S_{js}^{in}=\frac{GA_s}{L};\ S_{js}^{p}=\frac{K_s^h A_s}{L};\ S_{ja}^{in}=\frac{EA}{L};\ S_{ja}^{p}=\frac{K_a^h A}{L} \tag{1}$$

where E, G are Young's-like modulus and shear-like modulus, respectively; I, A_s, A are geometric characteristics of the cross section; $K_{M,1}^h, K_M^d\ K_s^h, K_a^h$ are hardening-like moduli; while L is the length of the beam.

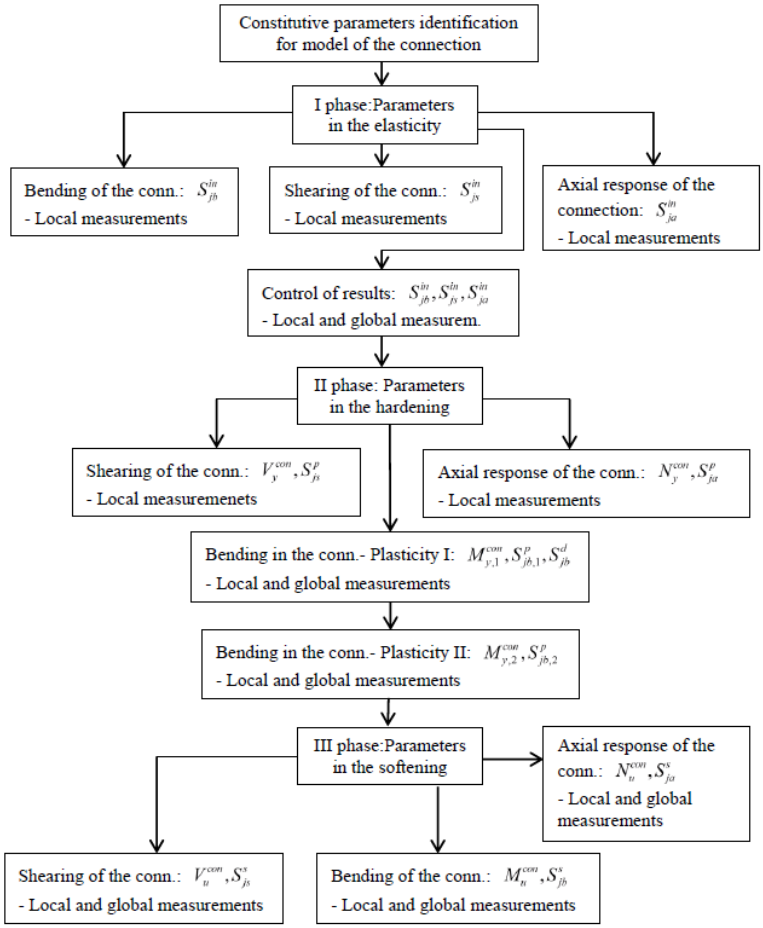

Fig. 16 Flowchart of parameters identification

For every case in the second and the third identification phase, local and global measurements are required. The local measurements depend mainly on one material parameter, while the global measurements depend on practically all parameters of constitutive models.

The standard algorithms for unconstrained minimization included in Matlab are sufficient to solve the identification problems for each and every phase. The key step to facilitate this is in a pertinent choice of the objective function for the parameters identification with the general format that can be written as (Imamovic *et al.* 2015)

$$\begin{aligned} J\left(\mathbf{d}_p\right) = & \sum_1^3 a\left(F_{Pi}^{com} - F_{Pi}^{\exp}\right)^2 + \sum_1^3 b\left(U_{Pi}^{com} - U_{Pi}^{\exp}\right)^2 + \sum_1^3 b\left(U_{S,Pi}^{com} - U_{S,Pi}^{\exp}\right)^2 \\ & + \sum_1^3 c\left(\theta_{Pi}^{com} - \theta_{Pi}^{\exp}\right)^2 + \sum_1^2 d\left(\Delta\theta_{Pi}^{com} - \Delta\theta_{Pi}^{\exp}\right)^2 + \sum_1^3 e\left(\kappa_{Pi}^{com} - \kappa_{Pi}^{\exp}\right)^2 \\ & + \sum_1^3 g\left(\Delta\kappa_{Pi}^{com} - \Delta\kappa_{Pi}^{\exp}\right)^2 \end{aligned} \tag{27}$$

where: $F_{Pi}^{com}, F_{Pi}^{\exp}$ are forces for different load level (P_i); $U_{Pi}^{com}, U_{Pi}^{\exp}$ are the corresponding displacements (P_i) ; $U_{S,Pi}^{com}, U_{S,Pi}^{\exp}$ are shear displacements (P_i); $\theta_{Pi}^{com}, \theta_{Pi}^{\exp}$ are rotations of the connection (P_i); $\Delta\theta_{Pi}^{com} = \theta_{Pi+1}^{com} - \theta_{Pi}^{com}$ and $\Delta\theta_{Pi}^{\exp} = \theta_{Pi+1}^{\exp} - \theta_{Pi}^{\exp}$ are gradients of rotation between two different load (P_i) ; $\kappa_{Pi}^{com}, \kappa_{Pi}^{\exp}$ are curvatures of the section (P_i); $\Delta\kappa_{Pi}^{com} = \kappa_{Pi+1}^{com} - \kappa_{Pi}^{com}$ and $\Delta\kappa_{Pi}^{\exp} = \kappa_{Pi+1}^{\exp} - \kappa_{Pi}^{\exp}$ are gradients of curvature between two different load (P_i); while *a, b, c, d, e, g* are constants.

By respecting experimental testing described in the second section of the paper, we are not able to identify parameters related to the axial force. However, we have exploited the design principle "strong columns - weak beams" in which the axial force behavior can be neglected. Some of the experimental measurements show that relative shear displacement between horizontal and vertical beams are too small. For these experimental tests, parameters related to shear force are not identified but assumed as rigid.

4.1 Experimental tests: A1 and A2

The experimental equipment in tests A1 and A2 (Figs. 4 and 5) has not measured relative shear displacement $U_{3,Pi}^{\exp}$. This fact reduces identification problem to seven unknowns, where all parameters are related to rotational response. In the first elastic phase, we have only one unknown constitutive parameter. In the second phase, four constitutive parameters are unknown, and only two parameters are unknown in the last third phase. The identification procedure uses the same objective function (27) for every case. In Figs. 17 and 18 are shown the shapes of the objective function for performed phases and cases of the identification.

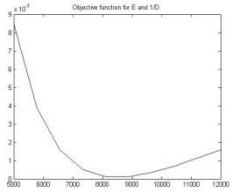

(a) Elasticity: S_{jb}^{in}

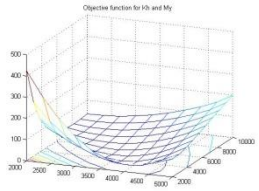

(b) Plasticity- first hardening: $M_{y,1}^{con}, S_{jb,1}^{p}$

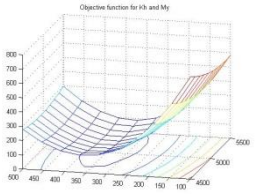

(c) Plasticity - second hardening: $M_{y,2}^{con}, S_{jb,2}^{p}$

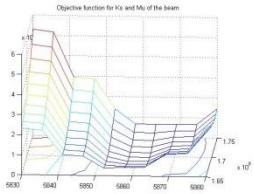

(d) Softening: M_{u}^{con}, S_{jb}^{s}

Fig. 17 Objective function shapes for eight unknowns related to bending - Experimental structure A1

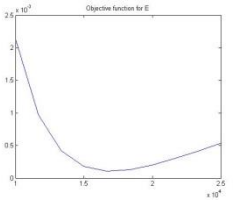

(a) Elasticity: S_{jb}^{in}

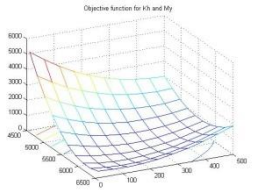

(b) Plasticity- first hardening: $M_{y,1}^{con}, S_{jb,1}^{p}$

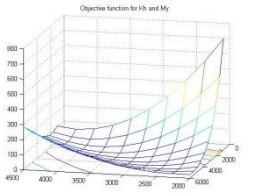

(c) Plasticity - second hardening: $M_{y,2}^{con}, S_{jb,2}^{p}$

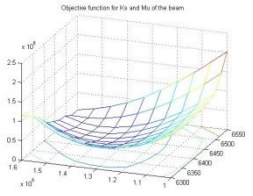

(d) Softening: M_{u}^{con}, S_{jb}^{s}

Fig. 18 Objective function shapes for eight unknowns related to bending - Experimental structure A2

In Tables 3 and 4, the values of identified constitutive parameters are shown and compared with the corresponding parameter values obtained by using the EC3 procedure.

Table 3 Values of the constitutive parameters for connection A1

	S_{jb}^{in} [kNm/rad]	S_{js}^{in} [kN/rad]	$M_{y,1}^{con}$ [kNm]	$S_{jb,1}^{p}$ [kNm/rad]	$M_{y,2}^{con}$ [kNm]	$S_{jb,2}^{p}$ [kNm/rad]	M_{u}^{con} [kNm]	S_{jb}^{s} [kNm/rad]	θ_c [rad]
Experiment	8235,3	∞	32,0031	3362,99	50,12	137,1	54,0937	-1699,99	0,0679
Eurocode 3	7506	-	26,25	2501,35	39,375	0	39,375	-	0,0165

Table 4 Values of the constitutive parameters for connection A2

	S_{jb}^{in} [kNcm/rad]	S_{js}^{in} [kN/rad]	$M_{y,1}^{con}$ [kNcm]	$S_{jb,1}^{p}$ [kNcm/rad]	$M_{y,2}^{con}$ [kNcm]	$S_{jb,2}^{p}$ [kNcm/rad]	M_{u}^{con} [kNcm]	S_{jb}^{s} [kNcm/rad]	θ_c [rad]
Experiment	8191,65	∞	31,15	3699,8	55,15	173,47	59,45	-1250,0	0,0755
Eurocode 3	7506	-	27,91	2501,35	41,87	0	41,87	-	0,01785

Results of the identification procedure are presented in Fig. 19 where we can see a good match between the experimental and the computed results. Computed results were obtained by using FEM model and identified constitutive parameters. Comparing the experimental response of the connection against the response predicted by EC3, we can see a fairly good match for the elastic response but a significant difference in load-bearing capacities of the connections. Namely, we have measured values of load-bearing capacities that are almost 44% higher than the corresponding values provided by EC3.

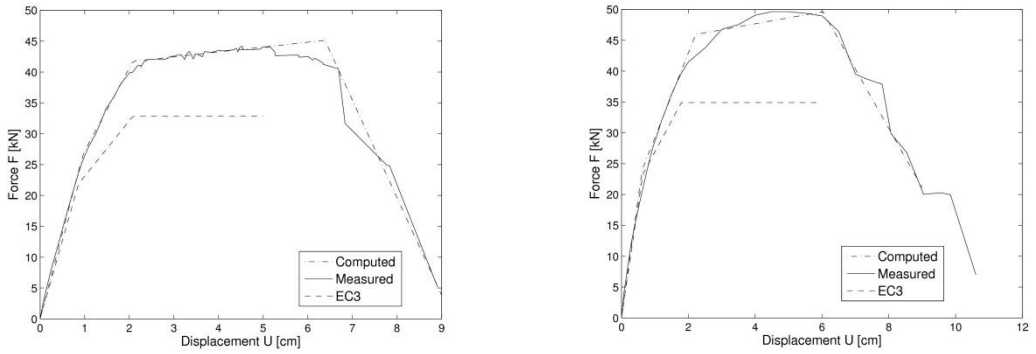

(a) Experimental structure A1 (b) Experimental structure A2

Fig. 19 Computed vs. Experimental responses of the connections: A1 and A2

4.2 Experimental tests: B1 and B2

The experimental responses (Figs. 8 and 9) of end plate connections (B1 and B2) show that shear displacement exists. Therefore, in this connection type, we have twelve unknowns, seven

related to bending moment and five related to shear force. The number of unknowns can be reduced to ten if we recall the assumption that failure of connection can happen due to the bending moment, or due to the shear force. Experimental measurements show that failures in both tests (B1 and B2) have happened due to the bending moment. In Figs. 20 and 21, shapes of the objective function (27) for the connections B1 and B2 are shown. In test B1 brittle failure happened where both bolts in tension zone broke at the same moment of time. Here, we are not able to identify the constitutive parameters related to the softening response since sudden drop occurs.

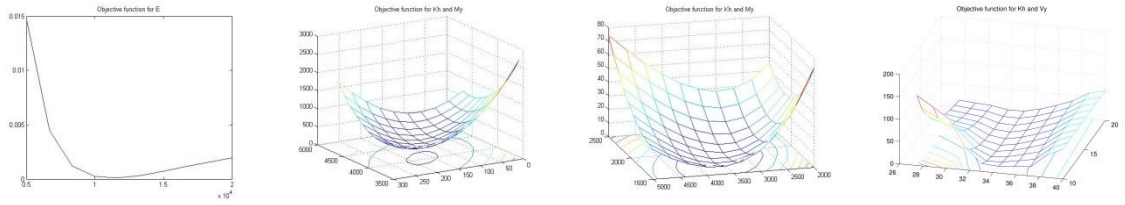

(a) Elasticity (bending): S_{jb}^{in} (b) Plasticity(bending) - first hardening: $M_{y,1}^{con}, S_{jb,1}^{p}$ (c) Plasticity(bending) - second hardening: $M_{y,2}^{con}, S_{jb,2}^{p}$ (d) Plasticity: V_y^{con}, S_{js}^{p} (shear force)

Fig. 20 Objective function shapes for ten unknowns - Experimental structure B1

Results of the identification are presented in Fig. 22, where we can see good matching between the experimental and the computed results. Computed results were obtained by using FEM model and identified constitutive parameters. Comparing the experimental responses of connections B1 and B2 against the EC3 responses, we can see a significant difference. Namely, we have measured almost 90% bigger load-bearing capacities of the connections than the corresponding capacities according to EC3.

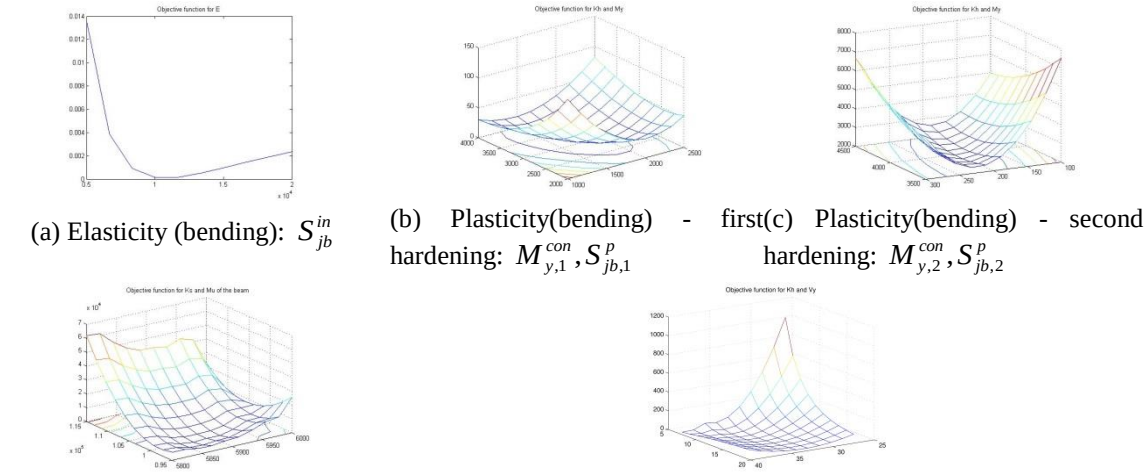

(a) Elasticity (bending): S_{jb}^{in} (b) Plasticity(bending) - first hardening: $M_{y,1}^{con}, S_{jb,1}^{p}$ (c) Plasticity(bending) - second hardening: $M_{y,2}^{con}, S_{jb,2}^{p}$ (d) Softening(bending): M_u^{con}, S_{jb}^{s} (c) Plasticity(shear force): V_y^{con}, S_{js}^{p}

Fig. 21 Objective function shapes for ten unknowns - Experimental structure B2

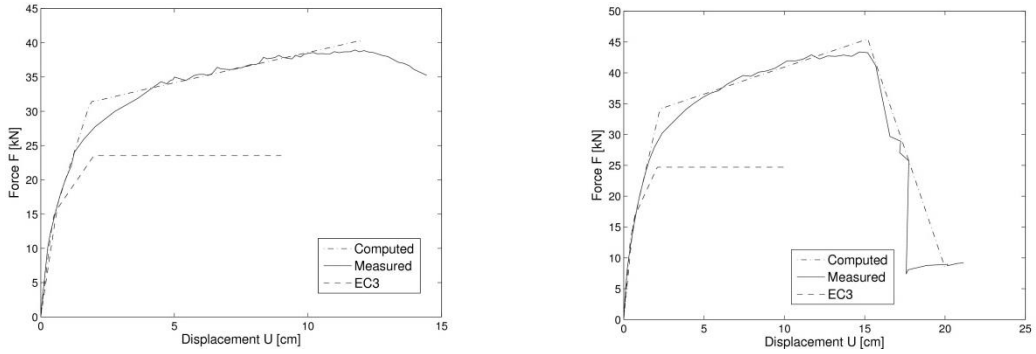

(a) Experimental structure B1 (b) Experimental structure B2

Fig. 22 Computed vs. Experimental responses of the connections: B1 and B2

The values of identified constitutive parameters are shown in Tables 5 and 6. These values are compared with the corresponding parameters obtained using the EC3 procedure. The EC3 procedure gives a very good prediction of the elastic response and bending of the connection.

According to EC3, the elastic response of this joint type can be assumed for the load values lower than the 66% of the load-bearing capacity. Experimental testing confirms this hypothesis.

Table 5 Values of the constitutive parameters for connection B1

	S_{jb}^{in}	S_{js}^{in}	$M_{y,1}^{con}$	$S_{jb,1}^{p}$	$M_{y,2}^{con}$	$S_{jb,2}^{p}$	V_{y}^{con}	S_{js}^{p}	M_{u}^{con}	θ_c
	[kNm/rad]	[kN/rad]	[kNm]	[kNm/rad]	[kNm]	[kNm/rad]	[kN]	[kN/m]	[kNm]	[rad]
Exp	5398,05	∞	16,88	3317,11	37,62	161,0	33,03	16102	54,0937	0,1161
EC3	3784	-	18,83	1260,24	28,25	0	-	-	28,25	0,02384

Table 6 Values of the constitutive parameters for connection B2

	S_{jb}^{in}	S_{js}^{in}	$M_{y,1}^{con}$	$S_{jb,1}^{p}$	$M_{y,2}^{con}$	$S_{jb,2}^{p}$	V_{y}^{con}	S_{js}^{p}	M_{u}^{con}	S_{jb}^{s}	θ_c
	[kNm/rad]	[kN/rad]	[kNm]	[kNm/rad]	[kNm]	[kNm/rad]	[kN]	[kN/m]	[kNm]	[kNm/rad]	[rad]
Exp	5165,25	∞	16,47	2939,10	38,11	217,21	35,17	21721	54,40	-1043,67	0,1651
EC3	3784	-	19,75	1260,24	29,625	0	-	-	29,625	-	0,0251

4.3 Experimental tests: A3 and B3

The structural connections A3 and B3 are completely the same as structural connections A1 and B1, which were presented in the previous sections. At the beginning of the identification process, we match the experimentally measured cyclic responses of structural connections with the numerically obtained responses. The numerical computations for the case of the monotonic loading, are performed with the proposed beam model using previously identified constitutive parameters from experimental structures A1 and B1 (see Fig. 23).

From the results shown in Fig. 23, we can conclude that good matching between the computed response and the contour of the hysteresis is obtained. That validates previously identified

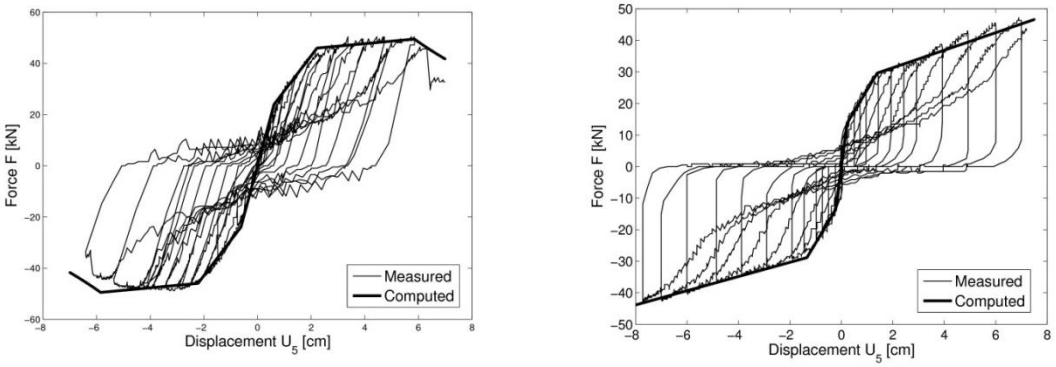

(a) A3 connection (b) B3 connection

Fig. 23 Computed vs. Experimental responses of the connections: A3 and B3

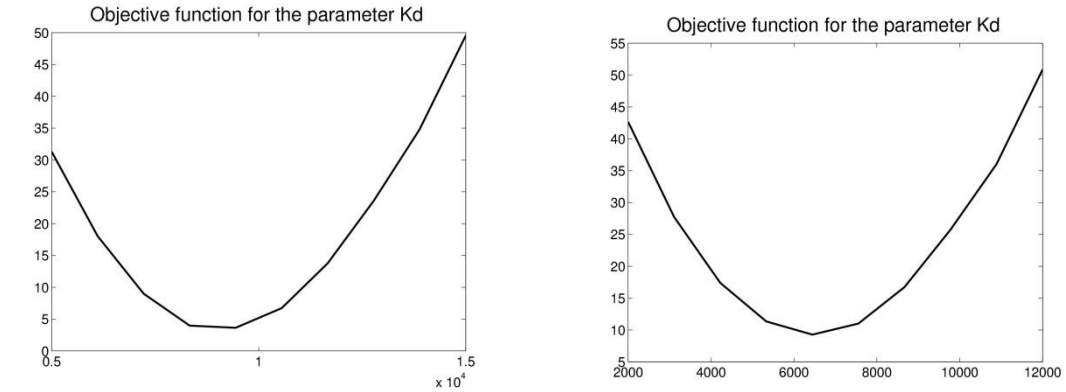

(a) Experimental structure A3 (b) Experimental structure B3

Fig. 24 The shape of the objective function

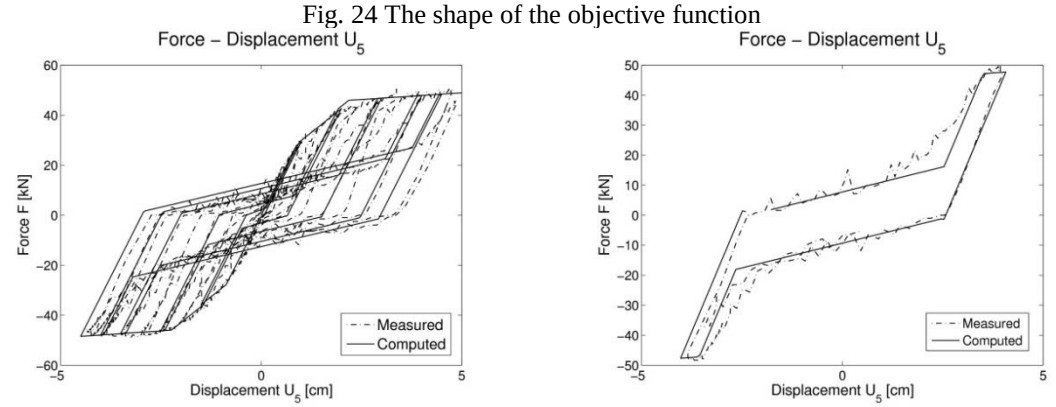

(a) Hysteresis (b) One cycle of the hysteresis

Fig. 25 Computed vs. Measured response of the experimental structure A3

constitutive parameters. The experimental observation has inspired assumption that the damage is beginning at the same moment as the plasticity. This assumption reduces identification problem to only one unknown per each connection.

Fig. 24 shows shapes of the objective function (27) for unknown parameters related to damage model. The shapes of the objective function are convex which thus have a minimum. By using the presented identification procedure, we are able to determine the unknown parameters.

By using the identified parameter, we have performed the numerical simulation of the experimental test A3. The comparison of the computed and the measured response is shown in Fig. 25. In Fig. 25(a) the computed and the measured hysteresis are shown. One extracted cycle is shown in Fig. 25(b). Both of them indicate that proposed model is capable of representing the connection behavior, including many phenomena characteristic for this structural connection type.

The numerical simulation of the cyclic experimental test B3 has been performed with the proposed beam element and identified parameters. Fig. 26 shows a comparison of computed and measured responses of the experimental structure B3, under cyclic loading. The difference between responses is visible, but we can conclude that proposed beam model significantly improves the response prediction in comparison with the model of the plasticity or the damage.

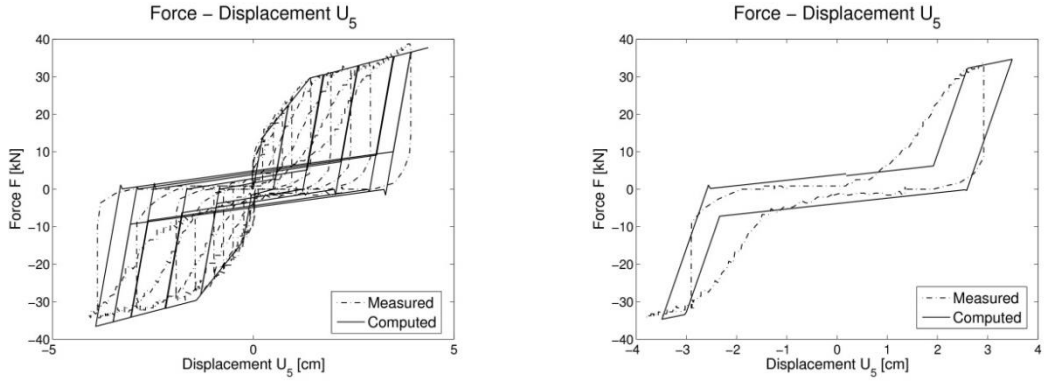

(a) Hysteresis (b) One cycle of the hysteresis

Fig. 26 Computed vs. Measured response of the experimental structure B3

5. Numerical examples

Three numerical examples are presented in this section to illustrate the effects of connections behavior on the global steel frame structure response. The global response of the steel frame structure with included connection behavior is compared with the global response of the same steel frame structure without included connection behavior. The comparison quantifies the connection behavior influence on the global response of the structure. All numerical computations are performed with a research version of the computer program FEAP (Taylor 2008).

5.1 The ultimate analysis of a simple steel frame structure

In this example, we analyze the influence of the connection behavior on the structure response. We consider a simple steel frame shown in Fig. 27(a), where the span is 5,0 m and height is 3,0 m. The mesh is composed of 48 beam elements where the length of each element is 0,25 m. The material properties of all frame members are the same (Young's modulus: $E=2\cdot10^4$ kN/cm^2; hardening modulus: $K=0.05\cdot E$;). The geometric properties of the beam cross-section corresponds

to the profile IPE 200 (*Moment of Inertia: I=1940 cm^4; Area of cross section: A=28.5 cm^2; Yield bending moment: My=4655 kNcm; Ultimate bending moment: Mu=5280 kNcm; Yield shear force: V_y=252 kN; Ultimate shear force: V_u=378 kN, Fracture energies: $G_{f,M}$=550 and $G_{f,V}$=450*). The column properties are defined as profile IPE 300 (*Moment of Inertia: I=11770 cm^4; Area of cross section: A=53,8 cm^2; Yield bending moment: My=13368 kNcm; Ultimate bending moment: Mu=15080 kNcm; Yield shear force: V_y=471 kN; Ultimate shear force: V_u=707 kN, Fracture energies: $G_{f,M}$=650 and $G_{f,V}$=550*). Three numerical simulations have been performed. In the first simulation, elements which connect beams and columns are defined according to the behavior of the experimentally tested connection denoted with A1. The second analysis does not include connection behavior, while the third connection behavior is defined according to EC3 (EC3 2005). The results of these three simulations are compared in Fig. 27(b), where we can see a significant effect of connections on the global response of the structure under vertical load. This effect is particularly evident at the level of ultimate forces, close to bearing capacity of the structure. On the other side, the connection behavior according to EC3 significantly reduce load-bearing capacity and stiffness of the structure.

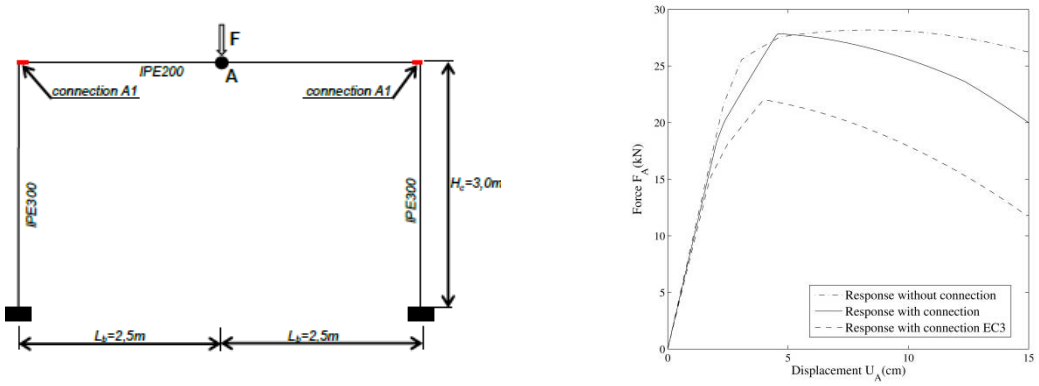

(a) Frame structure geometry (b) Response of the frame structure

Fig. 27 The simple steel frame

5.2 Pushover analysis of symmetric steel frame

In this example, we present the results of a push-over analysis of symmetric steel frame with and without included joints behavior. The frame geometry is given in Fig. 28(a). Material properties for all frame members are the same (Young's modulus: E=2·10^4 kN/cm^2; hardening modulus: K=0.05·E). The geometric properties of beams correspond to the profile IPE 200; the columns are defined as a profile IPE 300. In the first case, the constitutive parameters of elements which connect beams to columns are identified according to experimental test A1, whereas in the second case these elements are defined as a profile IPE 200. The vertical load was applied to all beam members. This load is kept constant throughout the pushover analysis to simulate the dead load effect. The lateral loading is applied regarding imposed incremental displacement (u_{top}) at the left upper corner (point A, see Fig. 28(a)).

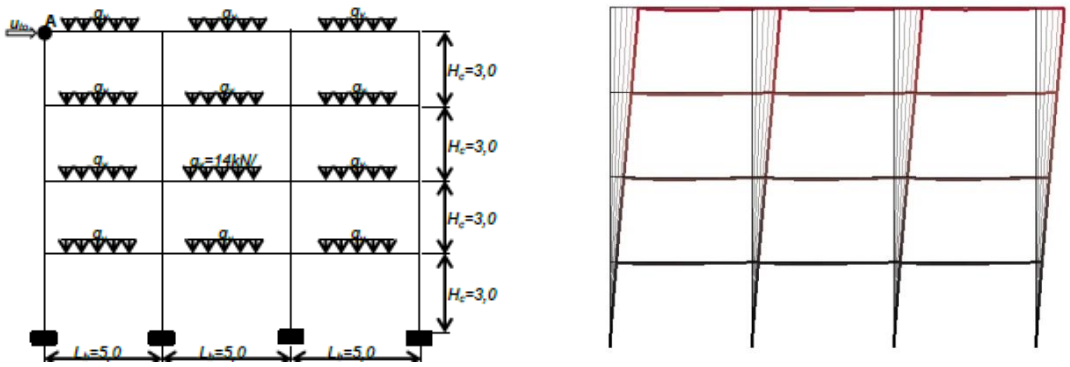

(a) The frame structure geometry (b) Deformed frame structure (step-by-step)

Fig. 28 The symmetric steel frame

The results of numerical simulations are shown in Fig. 29. These results show a significant influence of the connections behavior on the global response of steel frame structure. This effect is very evident at the level close to the ultimate load. The connections behavior reduces load bearing capacity and changes the global response of the steel structure. Namely, at the lateral displacement of 1 m, lateral resistance is reduced by 24% with regard to the structure without connections, while the connection behavior according to EC3 additionally reduces the lateral load-bearing capacity of structure up to 10%. Respecting these results, we can mark the importance of connection behavior in the steel structure design related to seismic load.

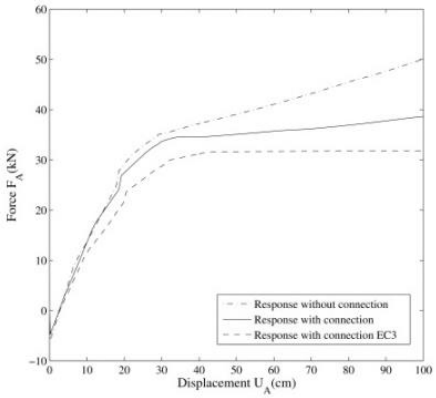

Fig. 29 Response of the symmetric frame structure

5.3 The steel frame response under cyclic loading

In this example, we illustrate the capability of representing connection behavior in the analysis of steel frame structure under cyclic loading. The structural connection behavior under cyclic loading is very complex and has a significant effect on the global response of steel frame structure. Furthermore, EC3 (EC3 2005) does not propose prediction procedure for this load type.

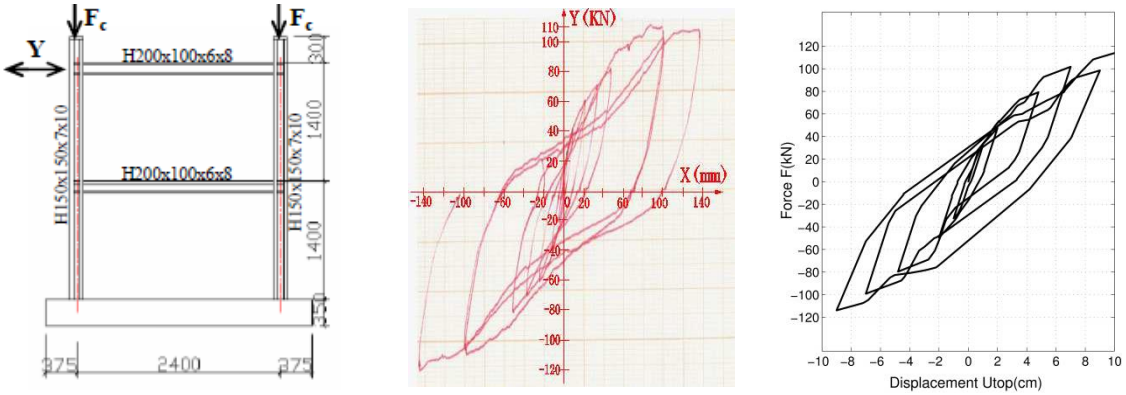

(a) Geometry and loads (Wang 2007) (b) Measured hysteresis (Wang 2007) (c) Computed hysteresis

Fig. 30 Experimental test of the steel frame structure

In order to verify proposed beam model, we have found an experimentally measured response of a steel frame structure with connections, which was tested under cyclic loading (Wang 2007). The tested two-story frame structure and loading are shown in Fig. 30(a). Forces $\boldsymbol{F_c}$ was kept as constant during the test in order to simulate dead load effect of above structure, while the force $\boldsymbol{Y}$ was applied as a cyclic load. The horizontal displacement of upper beam is denoted by $\boldsymbol{X}$(mm) in Fig. 30(b).

The experimental data presented in the paper are not sufficient for performing identification of constitutive parameters. Therefore we just compare shapes of the measured and the computed hysteresis (see Fig. 30). By comparing this two hysteresis, we can conclude that proposed beam model has the capability of representing steel frame response if we have sufficient measured data regarding connections behavior, which provides successful identification of model parameters.

6. Conclusions

In this paper we have presented an experimental and numerical study of the moment-resistant connection behavior, under monotonic and cyclic load. A total of two connection types have been analyzed and six experimental tests have been performed. The connection behavior in structural response is included where we model every joint with beam element. The proposed beam element has eighteen unknown constitutive parameters. The identification methodology has been presented and unknown parameters, based on the results of the experimental tests, have been identified. We found that the proposed beam model with identified constitutive parameters can successfully represent connection behavior, under monotonic and cyclic load. The capability of the proposed beam model to represent connection behavior is shown with very good match between experimental and computed results. The set of the constitutive parameters of the proposed beam model can be obtained by using the EC3 procedure, which provides a good prediction of elastic response and bending, while the plastic response prediction is overly conservative, sometimes up to 40%. The EC3 procedure doesn't predict connection behavior under cyclic load, while the proposed model and identification procedure are able to provide correct prediction and inclusion in

analysis of frame structure.

The influence of the connection behavior on the steel frame response is shown in three numerical simulations. The numerical results demonstrate the importance of the joints behavior on the steel frame structure response, where we can see a difference in results up to 30%. The effect of joints behavior completely changes response of steel frame structure under cyclic load, that is shown in third numerical simulation.

Acknowledgements

This work was supported by French Ministry of Foreign Affairs through a scholarship given by French Embassy in Sarajevo. This support is gratefully acknowledged.

References

Abidelah, B., A. and Kerdal, D.E. (2014), "Influence of the flexural rigidity of the bolt on the behavior of the T-stub steel connection", *Eng. Struct.*, **81**, 181-194.

EC3 (2005), *EN 1993-1-8: Eurocode 3: Design of Steel Structures - Part 1-8: Design of Joint*, Bruxelles: European Commitee.

Dujc, J., Bostjan, B. and Ibrahimbegovic, A. (2010), "Multi-scale computational model for failure analysis of metal frames that includes softening and local buckling", *Comput. Meth. Appl. Mech. Eng.*, **199**, 1371-1385.

Hill, R. (1950), *The Mathematical Theory of Plasticity*, Oxford: Clarendon Press.

Ibrahimbegovic, A. (2009), *Nonlinear Solid Mechanics*, Springer.

Ibrahimbegovic, A. and Frey, F. (1993a), "Finite element analysis of linear and non-linear planar deformations of elastic initially curved beam", *Int. J. Numer. Meth. Eng.*, **36**, 3239-3258.

Ibrahimbegovic, A., Knopf-Lenoir, C., Kučerova, A. and Villon, P. (2004), "Optimal design and optimal control of structures undergoing finite rotations and elastic deformations", *Int. J. Numer. Meth. Eng.*, **61**, 2428-60.

Imamovic, I., Ibrahimbegovic, A., Knopf-Lenoir, C. and Mesic, E. (2015), "Plasticity-damage model parameters identification for structural connections", *Coupled Syst. Mech.s*, **4**(4), 337-364.

Imamovic, I., Ibrahimbegovic, A. and Mesic, E. (2017), "Nonlinear kinematics Reissner's beam with combined hardening/softening elastoplasticity", *Comput. Struct.*, **189**, 12-20.

Kucerova, A., Brancherie, D., Ibrahimbegovic, A., Zeman, J. and Bittnar, Z. (2009), "Novel anisotropic continuum-discrete damage model capable of represenetnig localized failure of massive structures; part II: Identification from test under heterogeneous stress field", *Eng. Comput.*: *Int. J. Comput.-Aid. Eng. Softw.*, **1**(2), 128-144.

Nikolic, M., Ibrahimbegovic, A. and Miscevic, P. (2015), "Brittle and ductile failure of rocks: Embedded discontinuity approach for representing mode i and mode ii failure mechanisms", *Int. J. Numer. Meth. Eng.*, **8**(102).

Taylor, R.L. (2008), *FEAP - A Finite Element Analysis Program*, Berkeley.

Wagner. and Gruttmann, F. (2002), "Modeling of shell-beam transitions in the presence of finite rotations", *Comput. Assist. Mech. Eng. Sci.*, **9**, 405-418.

Wang, X. (2007), "Experimental research and finite element analysis on behavior of steel frame with semi-rigid connections", *Proceedings of the 5th WSEAS International Conference on Environment, Ecosystems and Development*, Tenerife, Spain, December.